Hybrid Density Functional Studies of the Oxidation of Phenol−Imidazole Hydrogen-Bonded Complexes: A Model for Tyrosine Oxidation in Oxygenic Photosynthesis

Patrick J. O'Malley

Contribution from the Department of Chemistry, UMIST, Manchester M60 1QD, U.K.

Received May 20, 1998. Revised Manuscript Received September 8, 1998

Abstract: Hybrid density functional calculations (B3LYP) show that one-electron oxidation of a phenol−imidazole hydrogen-bonded complex leads to spontaneous transfer of the phenolic proton to the imidazole, resulting in the formation of a phenoxyl radical−imidazolium ion complex. On comparison of the spin density distribution and hyperfine couplings, hydrogen bonding is shown principally to lead to a redistribution of spin density from the phenoxyl carbonyl oxygen atom to the carbonyl carbon atom. Loss of a proton from the phenoxyl−imidazolium ion results in a more loosely bound phenoxyl−imidazole complex, where a smaller spin redistribution is shown to occur on hydrogen bond formation. Comparisons between predicted hyperfine couplings for both hydrogen-bonded models and those reported for tyrosyl−histidine radical complexes involved in photosynthetic oxygen evolution indicate good agreement between experiment and theory.

Introduction

In green plant photosynthesis, photosystem II (PS II) drives the light-induced reduction of plasoquinone to plastoquinol resulting in the oxidation of water to oxygen.[1] Two tyrosine residues of the PS II complex are redox active. Using the amino acid numbering scheme for *Synechocystis* these are D2-Tyr160 (Y_D) and D1-Tyr161 (Y_Z). Y_Z forms a transient radical and appears to be directly involved in the electron-transfer reactions leading to oxygen evolution. Oxidation of Y_D, by contrast, forms a neutral tyrosyl radical which is stable in the dark and whose function is not clearly understood. Because of its stability, the Y_D radical has been well characterized by magnetic resonance[2−5] and FTIR[6,7] methods. It is currently speculated that D2-His189 is hydrogen-bonded to the reduced Y_D.[4,8] On oxidation of Y_D, it has been proposed that the phenolic proton is transferred to the imidazole group of this histidine. The transferred proton then hydrogen-bonds back to the tyrosyl radical oxygen.

The success of hybrid density functional methods in electronic structure determination was recently demonstrated. In particular, they are uniquely successful in describing large free radicals and intermolecular complexes.[9−14] In this study therefore we model the above events using hybrid density functional methods. The tyrosine residue is modeled by phenol, and the histidine residue is modeled by imidazole (Figure 1). We show that oxidation of the hydrogen-bonded phenol−imidazole complex leads spontaneously to transfer of the phenolic proton to the imidazole, resulting in a phenoxyl−imidazolium ion complex.

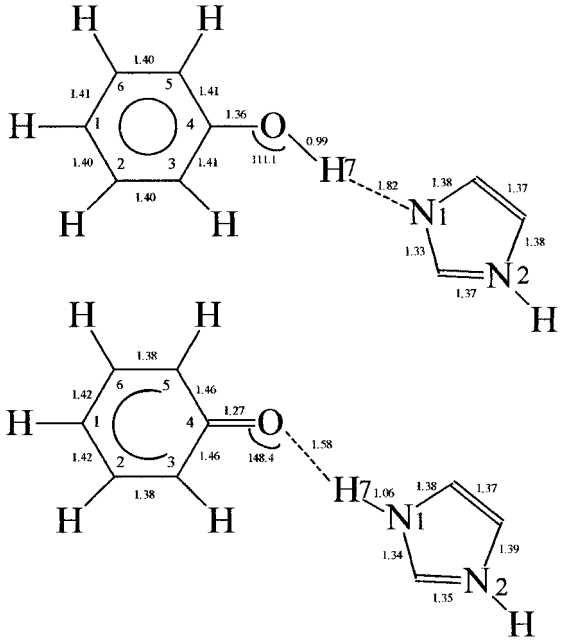

Figure 1. Effect of oxidation on the geometry of the phenol−imidazole complex; C_s point group: (top) reduced state; (bottom) oxidized form. Bond distances are given in angstroms; angles in degrees.

(1) *Oxygenic Photosynthesis: The Light Reactions*; Ort, D., Yocum, C., Eds.; Kluwer Academic Publishers: Dordrecht, The Netherlands, 1996.
(2) Babcock, G. T.; Sauer, K. *Biochim. Biophys. Acta* **1973**, *325*, 483.
(3) Rigby, S. E. J.; Nugent, J. H. A.; O'Malley, P. J. *Biochemistry* **1994**, *33*, 1734.
(4) Force, D. A.; Randall, D. W.; Britt, R. D.; Tang, X.-S.; Diner, B. A. *J. Am. Chem. Soc.* **1995**, *117*, 12643.
(5) Rigby, S. E. J.; Nugent, J. H. A.; McLachlan, D. J.; O'Malley, P. J. *Biochim. Biophys. Acta* **1994**, *1188*, 318.
(6) Hienerwadel, R.; Boussac, A.; Breton, J.; Diner, B. A.; Berthomieu, C. *Biochemistry* **1997**, *36*, 14712.
(7) MacDonald, G. M.; Bixby, K. A.; Barry, B. A. *Proc. Natl. Acad. Sci. U.S.A.* **1993**, *90*, 11024.
(8) Campbell, K. A.; Peloquin, J. M.; Diner, B. A.; Tang, X.-S.; Chisholm, D. A.; Britt, R. D. *J. Am. Chem. Soc.* **1997**, *119*, 4787.
(9) O'Malley, P. J.; Collins, S. J. *Chem. Phys. Lett.* **1996**, *259*, 296.
(10) O'Malley, P. J. *Chem. Phys. Lett.* **1996**, *262*, 797.
(11) O'Malley, P. J. *J. Phys. Chem. A* **1997**, *101*, 6334.
(12) O'Malley, P. J. *J. Phys. Chem. A* **1997**, *101*, 9813.
(13) O'Malley, P. J. *J. Phys. Chem. A* **1998**, *102*, 248.
(14) (a) Adamo, C.; Barone, V. In *Recent Developments in Density Functional Methods*; Chong, D. P., Ed.;World Scientific Publishing: Singapore, 1997; Part II. (b) Himo, F.; Graslund, A.; Eriksson, L. E. *Biophys. J.* **1997**, *72*, 1556. (c) Qin, Y.; Wheeler, R. A. *J. Chem. Phys.* **1995**, *102*, 1689.

10.1021/ja981755x CCC: $15.00
Published on Web 10/29/1998

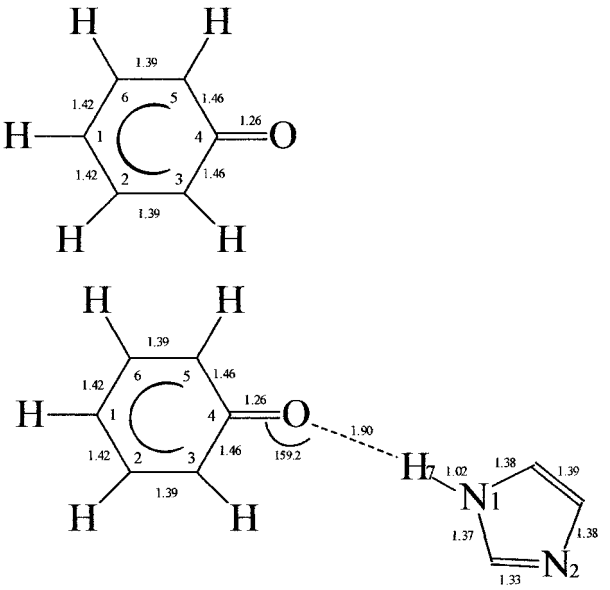

Figure 2. Bond distances and angles calculated for P(C_{2v}) and P−IM-(C_s).

The changes in spin density distribution brought about by hydrogen bond formation are analyzed, and ^{1}H, ^{13}C, and ^{17}O isotropic and anisotropic hyperfine couplings are calculated and compared with experimental determinations.

Methods

The complexes studied are given in Figures 1 and 2. The non-hydrogen-bonded phenoxyl radical is denoted P, phenoxyl hydrogen-bonded to imidazolium is denoted P−IMH, and phenoxyl hydrogen-bonded to imidazole is denoted P−IM. In addition, the unoxidized form of P−IMH, i.e. phenol hydrogen-bonded to imidazole, was also studied. All calculations were performed using the B3LYP hybrid density functional as implemented on Gaussian 94.[15] The EPR-II, double-ζ, basis set was used throughout.[16] Graphical analysis of spin densities was performed using SPARTAN.[17] Detailed procedures on the calculation of isotropic and anisotropic hyperfine couplings have been given in refs 9−11.

Results and Discussion

Geometries. The calculated geometries for the unoxidized and the oxidized P−IMH complexes are given in Figure 1. In Figure 2 the geometries of P and P−IM are also given for comparison.

Figure 1 demonstrates that one-electron oxidation results in spontaneous transfer of H7 from the phenol to the imidazole resulting in a phenoxyl−imidazolium ion complex. At the present level of theory, neither a non-proton-transferred form nor a transition state structure for proton transfer between phenol and imidazole could be found on the potential energy surface This suggests that, on oxidation of phenol−imidazole, therefore, the hydroxyl proton is transferred in a barrierless reaction path to lead to a phenoxyl radical interacting with an imidazolium ion. The unpaired electron is located on the phenoxyl portion as demonstrated by the 0.005 e/au^3 spin density surface in Figure 3. The adiabatic ionization potential calculated is 6.65 eV. This

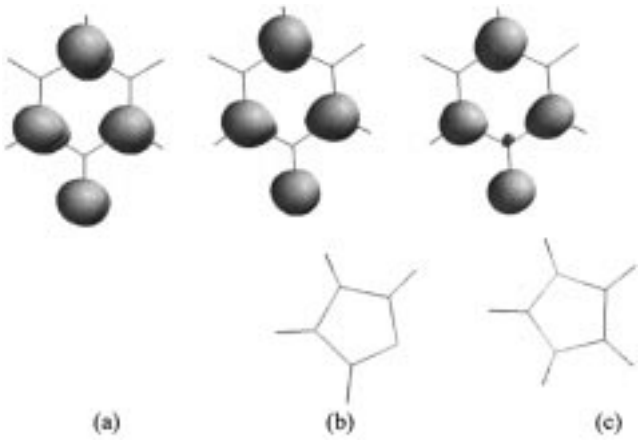

Figure 3. 0.005e/au^3 unpaired spin density surface contours: (a) P; (b) P−IM; (c) P−IMH.

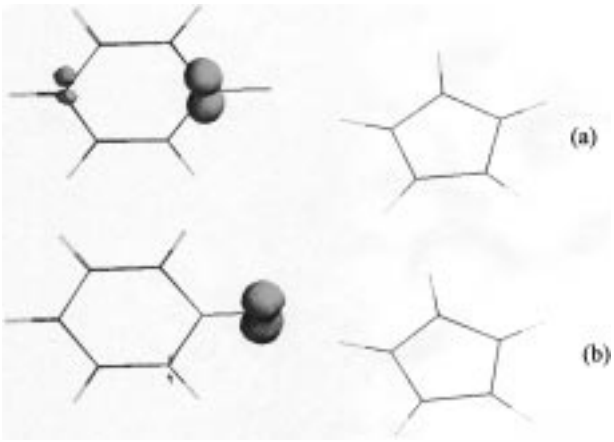

Figure 4. {P} − {P−IMH} difference spin density surface contours: (a) −0.006 e/au^3; (b) +0.006 e/au^3.

compares with the value of 8.16 eV calculated for ionization of isolated phenol to the phenol cation radical. Hydrogen bond formation with imidazole therefore lowers the ionization potential of phenol by 1.51 eV.

Figure 1 also demonstrates that oxidation leads to a more quinoid type geometry, i.e. a shortened CO bond and significantly increased C3C4 and C4C5 bond lengths, for the phenoxyl portion. On comparison with the geometries of P and P−IM (Figure 2), the phenoxyl internal geometries are quite similar. Removing the N2H proton from P−IMH results in P−IM leads to a significant increase in the O−H7 hydrogen bond length from 1.58 Å for P−IMH to 1.90 Å for P−IM. As expected, the positively charged hydrogen-bonded complex, P−IMH, is much more tightly bound.

Spin Densities. The positive 0.005 e/au^3 unpaired spin density surfaces for P, P−IMH, and P−IM are shown in Figure 3. The unpaired electron is clearly situated on the phenoxyl portion for all systems. Current attention is focused on the effect of hydrogen bonding on the phenoxyl-based tyrosyl radical in vivo,[4] and it is crucial to study the changes if any that occur in the spin density distribution on hydrogen bond formation. For this reason, in Figures 4 and 5 we present the difference spin density plots for {P} − {P−IMH}. The plots are presented at two isocontour values, 0.006 e/au^3 (Figure 4) and 0.002 e/au^3 (Figure 5). The more concentrated plot, Figure 4, reveals the major spin density changes occurring due to hydrogen bond formation whereas the second more diffuse plot, Figure 5, shows where additional smaller redistributions occur. The 0.006 e/au^3 difference contour in Figure 4 shows that the principal change

(15) Frisch, M. J.; Trucks, G. W.; Schlegel, H. B.; Gill, P. W.; Johnson, B. G.; Wong, M. W.; Foresman, J. B.; Robb, M. A.; Head-Gordon, M.; Replogle, E. S.; Gomperts, R.; Andres, J. L.; Raghvachari, K.; Binkley, J. S.; Gonzalez, C.; Martin, R. L.; Fox, D. J.; Defrees, D. J.; Baker, J.; Stewart, J. J. P.; Pople, J. A. *Gaussian 94*; Gaussian Inc.: Pittsburgh, PA, 1995.

(16) Barone, V. In *Recent Advances in Density Functional Methods*; Chong, D. P., Ed.; World Scientific Publishing: Singapore, 1995.

(17) *SPARTAN 4.1.1*; Wavefunction Inc.: Irvine, CA, 1995.

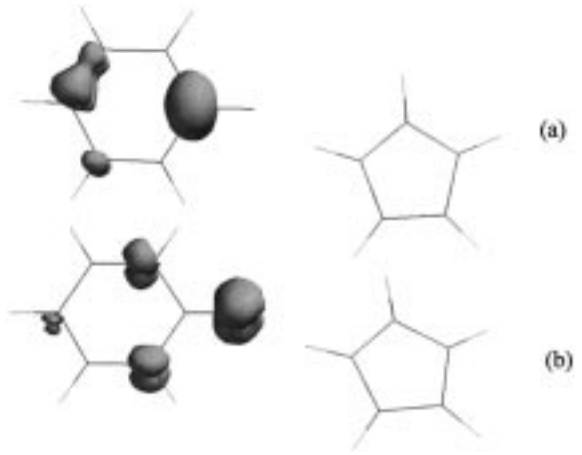

Figure 5. {P} − {P−IMH} difference spin density surface contours: (a) −0.002 e/au^3; (b) +0.002 e/au^3.

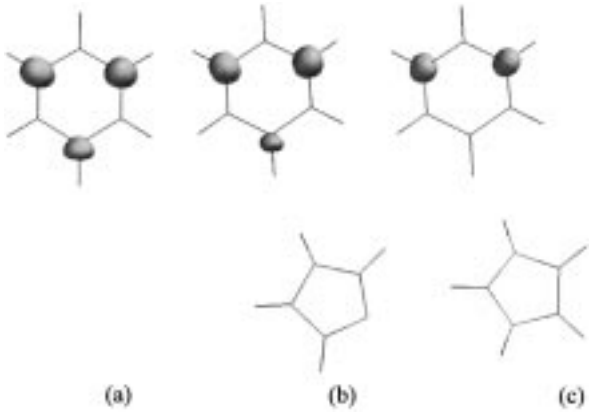

Figure 6. Negative, −0.005 e/au^3, spin density contours: (a) P; (b) P−IM; (c) P−IMH.

in spin density on hydrogen bond formation is a redistribution of spin density from the carbonyl oxygen atom to the carbonyl carbon atom. Using the more diffuse 0.002 e/au^3 difference contour, Figure 5, we can show that, on hydrogen bond formation, some spin density is lost from the C3 and C5 carbon atom positions and increases in spin density are noted at the C2 atom position and along the C1C6 bond. These changes in spin density distribution manifest themselves in the anisotropic and isotropic hyperfine coupling constants discussed below. The positive spin density plots mainly reflect the singly occupied molecular orbital, SOMO, distribution of the odd alternant phenoxyl. This gives rise to the high positive spin density at positions O, C3, C5, and C1 as demonstrated in Figure 3. Spin polarization by this α spin leads however to negative spin density at the formally nodal SOMO positions C4, C2, and C6 as shown by the −0.002 e/au^3 spin density contour in Figure 6. This figure also demonstrates the transfer of spin density to C4 on hydrogen bond formation as revealed above by the difference plots; Figure 6 shows that, for P, significant negative spin (excess β) is present at the C4 position. For P−IM, this has reduced in extent somewhat owing to the transfer of some positive spin from the oxygen atom position due to hydrogen bond formation. For P−IMH, we can see that, at this contour level, no negative spin is apparent at C4. Here the transfer of α spin to this position on hydrogen bond formation has reduced the negative spin at this position sufficiently to render it outside the −0.002 e/au^3 contour range. Indeed some positive spin density is evident at the C4 position from the positive spin density contours shown on Figure 3 indicating a slight excess of α spin at the C4 position for P−IMH.

^{13}C, ^{17}O, and ^{14}N Hyperfine Couplings. The anisotropic hyperfine couplings presented in Tables 1 and 2 are a direct reflection of the spin density contours in Figures 3−6. The magnitude and symmetry of the tensors reflect the spin density distribution already discussed. Large absolute and axial tensors are observed for the O, C1, C3, and C5 positions, reflecting the presence of positive unpaired π spin density at these positions. For C2, C6, and C4, the presence of negative spin density at these positions plus the presence of large positive values at neighboring positions distorts the picture somewhat, and the rhombic nature of the tensors reflects this fact. On hydrogen bond formation, the absolute values of the oxygen tensor decrease on going from P to P−IM to P−IMH. This reflects increasing hydrogen-bonding strength, accompanied by increasing transfer of spin density from the phenoxyl carbonyl oxygen to the phenoxyl carbonyl carbon in going from P−IM to P−IMH, as demonstrated in the difference spin density plots of Figures 4 and 5. As described above, most of this positive spin on the O atom position is transferred to C4. This reduces the net negative spin density at the C4 atom position, and this manifests itself in a gradual decrease in magnitude of the C4 anisotropic values on increasing hydrogen-bonding strength. A recent EPR study of the tyrosyl,Y_D, radical of photosystem II[18] reported the experimentally measured ^{17}O largest principal values. The total hyperfine tensor values reported are |121.1|, ≤ |19.6|, ≤ |19.6| MHz. The anisotropic and isotropic couplings derived from these values are also given in Table 1. Best agreement is observed with the P−IMH model although, considering the approximations involved, the agreement with the P−IM model values is also satisfactory. The absolute magnitudes of the C3 and C5 anisotropic tensors are also reduced on hydrogen bond formation, again reflecting the decrease in spin density at these positions revealed above. For the C2 and C6 positions, the absolute anisotropic values are decreased slightly, in particular the C6 tensor values. This is due again to the decrease in negative spin at these positions on hydrogen bond formation, in particular at the C6 atom position.

The isotropic couplings arise from spin density directly at the nuclei in question. This spin itself arises from spin polarization by the π spin. In general, spin polarization by an atom's own π spin gives rise to a positive spin density at the nucleus whereas spin polarization by a neighboring π spin gives rise to a negative contribution to the isotropic coupling. For ^{13}C and ^{1}H, which have positive magnetic moments, positive spin density gives rise to positive hyperfine coupling.

No significant change in the C1 isotropic coupling is brought about by hydrogen bond formation (see Table 1). For the C2 and C6 positions, a slight decrease in the absolute value of the isotropic coupling is observed, reflecting the lower negative π spin density at these positions on hydrogen bond formation. Both C3 and C5 isotropic hyperfine couplings decrease for the hydrogen-bonded complexes, reflecting the lower π spin density at these atom positions for the hydrogen-bonded complexes. The largest change in isotropic hyperfine coupling occurs for the C4 atom: from −38.2 MHz for P to −25.2 MHz for P−IMH. As discussed above, there is significantly more α spin at the C4 position for the hydrogen-bonded complexes, in particular P−IMH. The spin density leading to the isotropic hyperfine coupling of C4 arises there principally from spin polarization by its own π spin density and also from spin

(18) Dole, F.; Diner, B. A.; Hoganson, C. W.; Babcock, G. T.; Britt, R. D. *J. Am. Chem. Soc.* **1997**, *119*, 11540.

Table 1. ^{17}O, ^{13}C, and ^{14}N Anisotropic and Isotropic Hyperfine Coupling Constants Calculated for the Radical Complexes of Figures 1 and 2[a]

EXPT(Y_D)		ATOM	P		P-IM		P-IMH	
T_{11} T_{22} T_{33}	A_{iso}		T_{11} T_{22} T_{33}	A_{iso}	T_{11} T_{22} T_{33}	A_{iso}	T_{11} T_{22} T_{33}	A_{iso}
-93.8	-27.3	O	-123.5	-24.5	-115.0	-26.0	-100.0	-25.8
46.9			61.7		57.5		49.9	
46.9			61.8		57.6		50.2	
		C1	56.7	35.7	58.0	35.9	60.6	36.0
			-27.2		-27.9		-29.3	
			-29.5		-30.1		-31.3	
		C2	10.4	-27.5	10.0	-27.0	8.3	-24.7
			8.3		8.0		6.6	
			-18.7		-18.0		-14.9	
		C3	43.7	23.9	42.6	22.5	37.9	18.2
			-21.3		-20.6		-18.2	
			-22.4		-21.9		-19.7	
		C4	9.3	-38.2	6.1	-34.0	5.3	-25.2
			2.8		0.5		-0.5	
			-12.0		-6.6		-4.7	
		C5	43.7	23.9	42.7	22.7	39.6	19.5
			-21.3		-20.7		-19.1	
			-22.4		-22.0		-20.5	
		C6	10.4	-27.5	10.0	-27.0	9.0	-25.5
			8.3		8.1		7.3	
			-18.7		-18.1		-16.3	
0.0	|0.6|	N1	-	-	0.1	-0.4	0.1	-1.2
0.0			-		0.0		0.0	
0.0			-		-0.1		-0.1	
		N2	-	-	0.0	0.0	-0.1	0.1
			-		0.0		0.0	
			-		0.0		0.0	

[a] Experimental Y_D data are derived from values given in refs 8 and 18. All values are given in MHz.

polarization by its neighbors, i.e. O and C3/C5. The large negative value observed for isolated phenoxyl, P, is therefore a result of spin polarization by its own negative π spin and the positive π spin on O, C3, and C5. All will lead, via spin polarization, to negative spin density at the C4 nucleus, resulting in the large negative isotropic hyperfine coupling calculated. On hydrogen bond formation, the negative π spin at the C4 atom is decreased (Figure 5), which will lead to an increased (less negative) isotropic coupling. In addition, hydrogen bonding results in a decrease in the positive spin density at the O and C3/C5 positions, which will again lead to an increase in the isotropic hyperfine coupling of the C4 nucleus because of diminished spin polarization for these atoms.

Of particular significance is the prediction of sizable isotropic couplings for the N1 imidazole atom of P−IM and P−IMH. The absence of any significant anisotropic hyperfine couplings for N1 suggests that this presence of finite spin at the N1 nucleus is due to spin polarization through the hydrogen bond from the substantial π spin present on the O atom. As expected, this is substantially greater for the stronger hydrogen bond present in P−IMH. It is of particular note that a purely isotropic ^{15}N coupling was recorded recently for the tyrosyl, Y_D, radical of photosystem II.[8] It was shown that a hydrogen bond between the tyrosyl radical and histidine residue 189 is present with an interaction similar to that modeled here by P−IM or P−IMH. The experimental coupling was also shown to be essentially isotropic, which is again in agreement with the near-zero anisotropic couplings calculated for N1 (Table 1). The magnitude of the ^{15}N coupling measured in vivo translates into an ^{14}N hyperfine coupling of |0.6| MHz. This is somewhat closer to the P−IM model value of −0.4 MHz as opposed to the P−IMH value of −1.2 MHz. Increasing the hydrogen bond length for P−IMH (Table 3) (see discussion below) does reduce the magnitude of the N1 coupling for P−IMH, however.

^{1}H Hyperfine Couplings. ^1H hyperfine couplings are also reported in Table 2. The variation of the ring ^1H values with hydrogen bonding is much smaller than that of the heavier atom data. In this regard, it is perhaps unfortunate that only ^1H hyperfine data are readily amenable to experimental investigation. For the ring protons H2/H6 and H3/H5, a decrease in the

Table 2. ^{1}H Total (Anisotropic + Isotropic) and Isotropic Hyperfine Coupling Constants Calculated for the Radical Complexes of Figures 1 and 2[a]

EXPT(Y_D)	ATOM	P		P-IM		P-IMH	
A_{11} A_{22} A_{33}		A_{11} A_{22} A_{33}	A_{iso}	A_{11} A_{22} A_{33}	A_{iso}	A_{11} A_{22} A_{33}	A_{iso}
7.7 4.4 -	H2	12.0 6.5 5.0	7.8	11.4 6.3 4.6	7.4	9.5 5.2 3.1	6.0
-8.0 -19.1 -25.6	H3	-7.6 -22.2 -29.5	-19.8	-7.1 -21.8 -29.0	-19.3	-5.7 -19.9 -26.4	-17.3
- - -	H1	-9.1 -26.1 -40.6	-25.3	-9.2 -26.8 -41.4	-25.8	-9.2 -28.2 -42.9	-26.8
-8.0 -20.5 -27.5	H5	-7.6 -22.2 -29.5	-19.8	-7.2 -21.9 -29.1	-19.4	-6.1 -20.8 -27.4	-18.1
7.4 4.8 -	H6	12.0 6.5 5.0	7.8	11.5 6.3 4.6	7.5	10.2 5.7 3.6	6.5
7.4 -3.7 -3.7	H7	- - -	-	8.5 -3.3 -4.0	0.4	10.7 -4.9 -6.5	-0.3

[a] Experimental Y_D data are derived from values given in refs 3 and 4. All values are given in MHz.

Table 3. Dependence of O, N1, and H7 Anisotropic and Isotropic Hyperfine Couplings on Hydrogen-Bonding Distance for the P−IMH Radical Complex of Figure 1[a]

	O-H7/angstroms					
	1.58(min)		1.8		1.9	
ATOM	T_{11} T_{22} T_{33}	A_{iso}	T_{11} T_{22} T_{33}	A_{iso}	T_{11} T_{22} T_{33}	A_{iso}
O	-100.0 49.9 50.2	-25.8	-104.1 51.8 52.3	-26.5	-105.6 52.6 53.1	-26.7
N1	0.1 0.0 -0.1	-1.2	0.1 -0.1 -0.1	-0.9	0.1 -0.1 -0.1	-0.8
H7	11.0 -4.7 -6.3	-0.3	8.4 -3.8 -4.6	0.0	7.4 -3.4 -4.0	0.0

[a] All values in MHz.

absolute hyperfine coupling values is noted on hydrogen bond formation. These proton hyperfine couplings are directly proportional to the spin density concentration at the neighboring carbon atoms, and the changes noted reflect the decrease in

positive spin density at C3/C5 and the decrease in negative spin density at C2/C6 brought about by hydrogen bond formation, as discussed above. The most noticeable difference between the ^{1}H data reported here and that reported previously for *p*-methylphenoxyl[19] is the much larger hydrogen bonding values of this study. For the *p*-methylphenoxyl−methylimidazolium complex in ref 19, the tensor principal values calculated using UB3LYP/EPRIII//PM3 for the hydrogen bonding proton were 8.2, −3.4, −3.6 MHz whereas the values reported here for P−IMH using UB3LYP/EPRII//UB3LYP/EPRII are significantly larger, i.e. 10.7, −4.9, −6.5 MHz. These differences are mainly attributable to the shorter hydrogen-bonding distance calculated for P−IMH in this study of 1.58 Å as opposed to 1.78 Å in the previous study. The principal difference between geometry optimization at the PM3 level and the density functional level is the prediction of a significantly longer hydrogen bond distance at PM3. While the PM3 method can give excellent internal geometries for phenoxyl radicals,[20,21] these data suggest that it overestimates hydrogen-bonding distances for such radicals. B3LYP is increasingly being shown to furnish highly accurate intermolecular hydrogen-bonding distances,[14,22] and as such the density functional hydrogen-bonding distance reported here must be considered more reliable. For the Y_D radical of photosystem II, deuterium exchange experiments, principally on manganese-depleted photosystem II complexes, have been used to detect exchangeable protons which have been assigned to the D2-His189 hydrogen-bonded proton.[4,23] In the most recent study,[4] an ENDOR band assigned to the axial component of the presumed purely dipolar hyperfine tensor was observed with a hyperfine coupling value of 3.7 MHz. This suggests hydrogen-bonded proton tensor values of 7.4, −3.7, and −3.7 MHz, and these values are given in Table 2. While these values lie close to the values we predicted in ref 19, they deviate significantly from the values predicted for P−IMH of this study. The predicted P−IMH values of Table 2 are 10.7, −4.9, and −6.5 MHz. Somewhat better agreement with experimental tyrosyl values is observed with the P−IM data of Table 2. One explanation for the difference between P−IMH calculated and tyrosyl Y_D experimental values may be that, in the protein environment, the hydrogen-bonding distance is constrained to be somewhat larger than the optimal value predicted here for the gas-phase complex. If we examine the O−N1 distance in Figure 1 we find a distance of 2.8 Å for the unoxidized form as opposed to 2.6 Å for the oxidized radical complex. In the protein environment, it is likely that the O and N atoms are constrained in their positions and the optimally shorter hydrogen-bonding distance for the oxidized form is not achieved. Table 3 shows the effect of increasing the hydrogen bond lengths to 1.8 and 1.9 Å on the calculated hyperfine couplings of P−IMH. The major effect of lengthening the hydrogen bond length for P−IMH is to reduce the hydrogen-bonded ^{1}H tensor values, resulting in closer agreement with the experimental hydrogen-bonding values observed for the Y_D radical of photosystem II.

Conclusions

Hybrid density functional calculations (B3LYP) show that one-electron oxidation of a phenol−imidazole hydrogen bonded complex leads to spontaneous transfer of the phenolic proton to the imidazole, resulting in the formation of a phenoxyl radical−imidazolium ion complex. The resulting phenoxyl−imidazolium and phenoxyl−imidazole radical complexes exhibit hyperfine coupling constants in remarkably good agreement with those determined for tyrosyl radicals involved in the oxygen evolution complex of photosystem II.

JA981755X

(19) O'Malley, P. J.; Ellson, D. A. *Biochim. Biophys. Acta* **1997**, *1320*, 65.

(20) O'Malley, P. J.; MacFarlane, A. J.; Rigby, S. E. J.; Nugent, J. H. A. *Biochim. Biophys. Acta* **1995**, *1232*, 175.

(21) Chipman, D. M.; Liu, R.; Zhou, X.; Pulay, P. *J. Chem. Phys.* **1994**, *100*, 5023.

(22) Sodupe, M.; Oliva, A.; Bertran, J. *J. Phys. Chem. A* **1997**, *101*, 9142.

(23) Rodriguez, I. D.; Chandrashekar, T. K.; Babcock, G. T. In *Progress in Photosynthesis Research*; Biggins, J., Ed.; Martinus Nijhoff: Dordrecht, The Netherlands, 1987; pp 471−474.